Stem Cell Reports
Article

OPEN ACCESS

PSA-NCAM-Negative Neural Crest Cells Emerging during Neural Induction of Pluripotent Stem Cells Cause Mesodermal Tumors and Unwanted Grafts

Dongjin R. Lee,[1] Jeong-Eun Yoo,[1] Jae Souk Lee,[1] Sanghyun Park,[1] Junwon Lee,[1] Chul-Yong Park,[1] Eunhyun Ji,[1] Han-Soo Kim,[2] Dong-Youn Hwang,[3] Dae-Sung Kim,[4,*] and Dong-Wook Kim[1,*]

[1]Department of Physiology and Brain Korea 21 PLUS Project for Medical Science, Yonsei University College of Medicine, Seoul 120-752, Korea
[2]Cell Therapy Center and Department of Laboratory Medicine, Yonsei University College of Medicine, Seoul 120-752, Korea
[3]Department of Biomedical Science, College of Life Science, CHA University, Seongnam, Gyeonggi-do 463-840, Korea
[4]Division of Biotechnology, College of Life Sciences and Biotechnology, Korea University, Seoul 136-713, Korea
*Correspondence: sonnet10@korea.ac.kr (D.-S.K.), dwkim2@yuhs.ac (D.-W.K.)
http://dx.doi.org/10.1016/j.stemcr.2015.04.002

SUMMARY

Tumorigenic potential of human pluripotent stem cells (hPSCs) is an important issue in clinical applications. Despite many efforts, PSC-derived neural precursor cells (NPCs) have repeatedly induced tumors in animal models even though pluripotent cells were not detected. We found that polysialic acid-neural cell adhesion molecule (PSA-NCAM)$^-$ cells among the early NPCs caused tumors, whereas PSA-NCAM$^+$ cells were nontumorigenic. Molecular profiling, global gene analysis, and multilineage differentiation of PSA-NCAM$^-$ cells confirm that they are multipotent neural crest stem cells (NCSCs) that could differentiate into both ectodermal and mesodermal lineages. Transplantation of PSA-NCAM$^-$ cells in a gradient manner mixed with PSA-NCAM$^+$ cells proportionally increased mesodermal tumor formation and unwanted grafts such as PERIPHERIN$^+$ cells or pigmented cells in the rat brain. Therefore, we suggest that NCSCs are a critical target for tumor prevention in hPSC-derived NPCs, and removal of PSA-NCAM$^-$ cells eliminates the tumorigenic potential originating from NCSCs after transplantation.

INTRODUCTION

In a process of attempting to mimic primary neuralization in vivo, studies have focused their attention on differentiating neural precursor cells (NPCs) from pluripotent stem cells (PSCs) for basic research and biomedical applications (Conti and Cattaneo, 2010). Given their advantages of a long-term expansion, high-culture purity, long-term neurogenic potentials, and their ability to survive cryopreservation, NPCs from human (h)PSC-derived neural rosettes, which represent neuroepithelial cells of unclosed and closed neural tubes, are an ideal cell source for biomedical applications (Chambers et al., 2009; Elkabetz et al., 2008; Koch et al., 2009). Unfortunately, however, there have been reports of tumor formation after transplantation even in the absence of undifferentiated PSCs. Two distinctive types of tumors have been mainly described: neural overgrowth and mesodermal tumors. Neural rosettes (early NPCs) possess self-renewing multipotent characteristics, and a previous study showed neural overgrowth when they were transplanted in vivo (Elkabetz et al., 2008). Subsequent studies overcame this tumorigenic potential by further committing primitive NPCs to specific cell types and increasing differentiation efficiency (Kirkeby et al., 2012; Kriks et al., 2011; Liu et al., 2013). Despite efforts to avoid pluripotent cell contamination and NPC-neural overgrowth, researchers continue to report tumor formation post-transplantation of human embryonic stem cell (hESC)-derived NPCs or neuronal precursor cells in animal models of CNS disorders containing chondrocytes, muscle fibers (Arnhold et al., 2004), mesoderm-derived mature cartilage (Seminatore et al., 2010), and pigmented cells (Doi et al., 2012).

Meanwhile, in vitro studies of neural induction from hPSCs have suggested that radial arrangements of columnar neuroepithelial cells, termed neural rosettes, can differentiate toward peripheral nervous system (PNS) lineages (Chambers et al., 2009; Kim et al., 2010) and reported evidence of neural crest-like cells within the neural rosette cultures (Elkabetz et al., 2008; Kim et al., 2012; Lee et al., 2007). During embryonic development, transient and highly migratory neural crest stem cells (NCSCs) give rise to melanocytes, neurons and glial cells of PNS, as well as connective tissue cells, chondrocytes, osteocytes, and adipocytes of the craniofacial complex (Le Douarin and Dupin, 2003). Neural crest cells share the same developmental origin of gastrula ectoderm as the neuroectoderm and hold multipotency yielding cells of mesodermal and ectodermal lineages that comprise the PNS (Knecht and Bronner-Fraser, 2002); therefore, we hypothesized that neural rosette cultures could be heterogeneous and may contain NCSCs that may cause mesodermal tumor growth and introduce unwanted cell populations (e.g., pigmented cells) after transplantation into the CNS.

In examining the heterogeneity of neural rosettes, we identified a subset (~21%) of PSA-NCAM$^-$ cells.

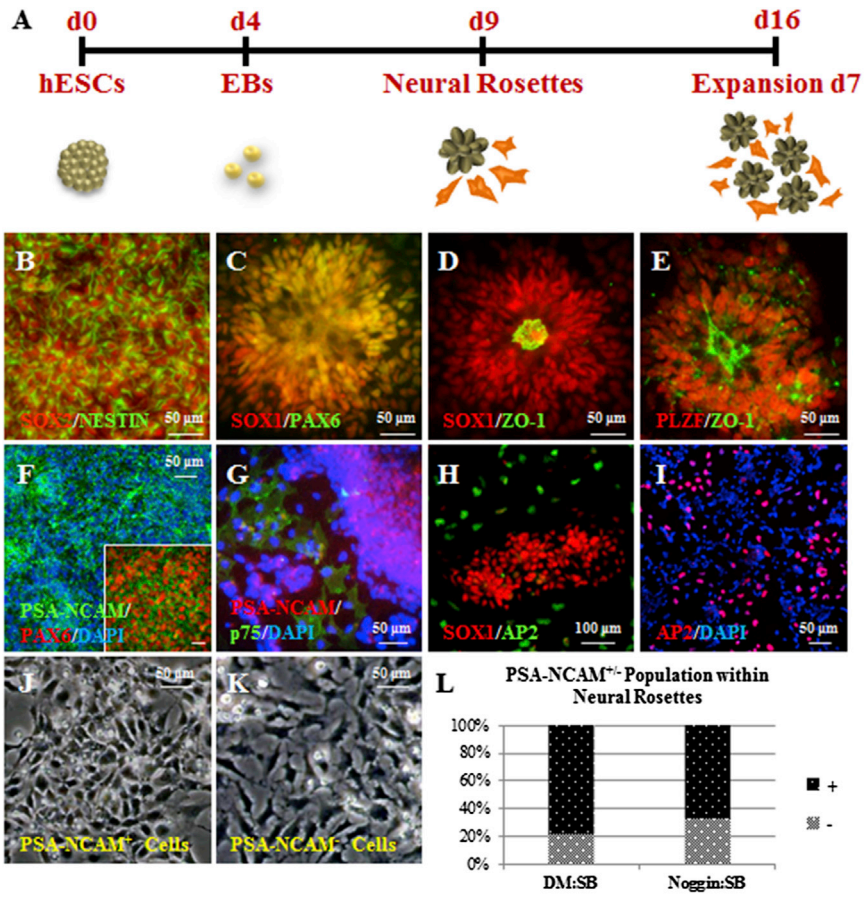

Figure 1. PSA-NCAM-Targeted Cell Sorting Can Isolate Neural Crest-like Cells from Heterogeneous Neural Rosette Cultures

(A) Timeline of neural rosette generation method.

(B and C) SOX2$^+$/NESTIN$^+$ and SOX1$^+$/PAX6$^+$ neuroepithelial cells were observed in the expanded neural rosette cultures.

(D and E) Coexpression of SOX1/ZO-1 and PLZF/ZO-1 identified the physical property of neural rosettes.

(F) Predominant PSA-NCAM$^+$ expression within the neural rosette population that was comprised of PAX6$^+$ neuroepithelial cells.

(G) p75$^+$ cells were observed peripheral to the PSA-NCAM$^+$ neural rosette core.

(H) AP2$^+$/SOX1$^-$ cells were observed peripheral to the SOX1$^+$ neural rosette core.

(I) AP2$^+$ cells were identified at a single-cell level.

(J and K) PSA-NCAM$^+$ cells showed neural rosette morphologies, whereas negative cells exhibited neural crest-like physical characteristics.

(L) Among the neural rosette cultures, the populations that were positive and negative for PSA-NCAM comprised 79% and 21% (n = 4 independent experiments), respectively. Another common method for neural induction using Noggin and SB431542 yielded ~30% PSA-NCAM$^-$ cells (n = 4 independent experiments).

See also Figure S1.

Interestingly, these cells did not express an early marker of neuroectoderm (Pax6), but they possessed NCSC characteristics. When isolated from neural rosette populations, PSA-NCAM$^-$ cells showed pronounced multipotent phenotypes when directed to differentiate. Because PSA-NCAM$^-$ cells carry multipotency of NCSCs, we postulated that PSA-NCAM$^-$ cells were responsible for the formation of mesodermal tumors and unwanted grafts after hPSC-derived NPC transplantation. To test the hypothesis, we transplanted PSA-NCAM$^-$ cells mixed with PSA-NCAM$^+$ cells in a gradient manner in the rat brain. Our investigation revealed a proportional increase in mesodermal tumor formation, the appearance of pigmented cells, and PERIPHERIN$^+$ grafts in the brain. These results indicate that NCSCs classified as PSA-NCAM$^-$ cells can be a new target for tumor prevention in hPSC-derived-NPC-based therapy and that removal of PSA-NCAM$^-$ cells would prevent the introduction of mesodermal tumor and unwanted graft formations after NPC transplantation in the CNS.

RESULTS

PSA-NCAM-Targeted Cell Sorting Isolates Neural Crest-like Cells from Heterogeneous Neural Rosette Populations

Neural induction and neural rosette isolation from hPSCs were performed as described in our previous reports (Figure 1A) (Kim et al., 2010, 2012). The expanded neural rosette cultures expressed neuroectodermal and neuroepithelial markers, including sex-determining region Y-box 2 (SOX2), NESTIN, SOX1, and paired box protein 6 (PAX6) (Figures 1B–1D). Tight junction protein (ZO-1) and promyelocytic leukemia zinc finger (PLZF) expression confirmed the neural rosette characteristics (Figures 1D and 1E), and the previously defined "rosette-specific markers" were also maintained throughout expansion (Figure S1A) (Elkabetz et al., 2008). As previously described, the neural rosette cultures appeared to be mainly PSA-NCAM$^+$ and consisted of PAX6$^+$ neuroepithelial cells (Figure 1F) (Kim et al., 2012). Despite the predominant PSA-NCAM$^+$

expression within the cultures, negative cells were observed around the outer boundary of PSA-NCAM$^+$ rosette core, and these cells expressed the neural crest marker p75 (Figure 1G). Expression of AP2 (a neural crest lineage marker) was also observed in SOX1$^-$ cells scattered around SOX1$^+$/AP2$^-$ neural rosettes (Figure 1H). AP2$^+$ cells remained when the neural rosette cultures were dissociated into single cells to examine the characteristics of individual cells (Figure 1I). These results indicated that the neural rosette cells were heterogeneous in terms of having neural crest-like characteristics and could be divided into PSA-NCAM$^+$ and PSA-NCAM$^-$ populations.

The heterogeneous neural rosette cultures were divided into two different populations via magnetic-activated cell sorting (MACS) using PSA-NCAM antibodies. The potential presence of residual undifferentiated cells was examined prior to MACS; however, no PSCs were detected in the neural rosette population or the sorted cells (Figures S1B and S1C). PSA-NCAM$^+$ cells had the physical appearance of polarized neural rosette cells and made of 79% of the total neural rosette population, whereas PSA-NCAM$^-$ cells had the morphology of neural crest-like cells and account for the remaining 21% of the total population (n = 4; Figures 1J–1L). The percentage of culture population suggests that expanded neural rosette cultures contain approximately 21% PSA-NCAM$^-$ cells with a non-neural rosette appearance.

Molecular Characterization and Global Gene Expression Analysis of PSA-NCAM$^-$ Show NCSC Characteristics

We analyzed the composition of PSA-NCAM$^-$ cells more closely because they exhibit a neural crest-like cell morphology that is not observed in neural cells of the CNS. We first examined the percentage of cells from the neural crest lineage using three neural crest markers: p75, HNK1, and AP2. Flow cytometry showed that up to 95.8% (n = 4) of the PSA-NCAM$^-$ population was p75$^+$, whereas 96.8% of this population was HNK1$^+$ (Figures 2A and 2B). PSA-NCAM$^-$ cells derived from the human induced PSC (iPSC) line WT-iPSCEpi3 provided similar results (Figures S2A–S2D). According to the fluorescence-activated cell sorting (FACS) results, the pluripotent cell marker SSEA4 was not expressed in PSA-NCAM$^-$ cells (Figure 2C). Additionally, 86.9% of the initial passage (p0) of PSA-NCAM$^-$ cells were positive for AP2, and this increased to 92.3% as the cells were further subcultured (p2), suggesting progressive specification toward neural crest cells ($n = 3$, $p < 0.05$). The quantification of cells expressing Ki67, a cell-cycle marker for an all-active phase, showed that 88.9% of AP2$^+$ PSA-NCAM$^-$ cells were in a proliferative state (Figure 2D). Immunocytochemical analysis of the PSA-NCAM$^-$ cells verified their neural crest identities (Figures 2E–2H). To further characterize the PSA-NCAM$^-$ cells, we performed real-time RT-PCR analysis targeting key transcripts related to neural crest identity. PSA-NCAM$^-$ cells showed elevated levels of *p75* and *AP2* compared with neural rosette cells and PSA-NCAM$^+$ cells (Figures S3A and S3B). The expression level of *cMYC*, an important factor for pluripotency and the earliest expressed neural crest specifier (Prasad et al., 2012), was consistent throughout the targeted cells, with the exception of PSA-NCAM$^+$ cells (Figure S3C). PSA-NCAM$^-$ cells displayed elevated levels of transcripts responsible for premigratory and migratory NCSCs (Figures S3D–S3H), and the levels of epithelial-mesenchymal transition (EMT) regulatory factors such as *TWIST1*, *SLUG*, and *SNAIL* increased with the passage number (p2 versus p4) (Figures S3D–S3F) (Prasad et al., 2012). These results provide molecular evidence that multiple neural crest marker genes are predominantly expressed in PSA-NCAM$^-$ cells compared with PSA-NCAM$^+$ cells.

When isolating NCSCs from hPSCs in vitro, p75$^+$ or p75$^+$/HNK1$^+$ cells were targeted from differentiated cultures as described in previous reports (Chimge and Bayarsaihan, 2010; Jiang et al., 2009; Kreitzer et al., 2013; Lee et al., 2007; Menendez et al., 2011). Because we are providing the first evidence that PSA-NCAM$^-$ cells are NCSCs, we compared PSA-NCAM$^-$ cells to the previously established NCSCs, p75$^+$/HNK1$^+$ cells. Two step-MACS sorting was performed to obtain p75$^+$/HNK1$^+$ cells, and their purity was confirmed with flow cytometry and immunocytochemistry (Figures 2I–2L). Transcriptome analyses were performed in triplicate to compare the global gene expression patterns of neural rosettes, PSA-NCAM$^+$, PSA-NCAM$^-$, and p75$^+$/HNK1$^+$ cells (Figures 2M–2R). Hierarchical clustering analysis of 20,287 (fail count < 6) normalized genes was performed using complete linkage and Euclidean distance as measures of similarity. The expressed transcripts were clustered into two expression groups of neural rosettes and PSA-NCAM$^+$ cells versus PSA-NCAM$^-$ cells and p75$^+$/HNK1$^+$ cells (Figure 2M).

Next, we identified genes upregulated in PSA-NCAM$^+$, PSA-NCAM$^-$, and p75$^+$/HNK1$^+$ cells relative to neural rosettes (fold change >2.0). As shown in the Venn diagrams in Figure 2N, 1 gene in the PSA-NCAM$^+$ group, 104 genes in the PSA-NCAM$^-$ group, 67 genes in the p75$^+$/HNK1$^+$ group, and 143 genes in both the PSA-NCAM$^-$ group and the p75$^+$/HNK1$^+$ group were expressed at higher levels than in the neural rosette group (Table S1). Furthermore, we identified genes that were upregulated in PSA-NCAM$^-$ and p75$^+$/HNK1$^+$ cells relative to PSA-NCAM$^+$ cells (fold change >2.0). We found 113 genes in the PSA-NCAM$^-$ group, 56 genes in the p75$^+$/HNK1$^+$ group, and 144 genes in both the PSA-NCAM$^-$ and p75$^+$/HNK1$^+$ groups that were upregulated compared to the PSA-NCAM$^+$ group (Figure 2O). Gene Ontology (GO) analysis of the 257 genes

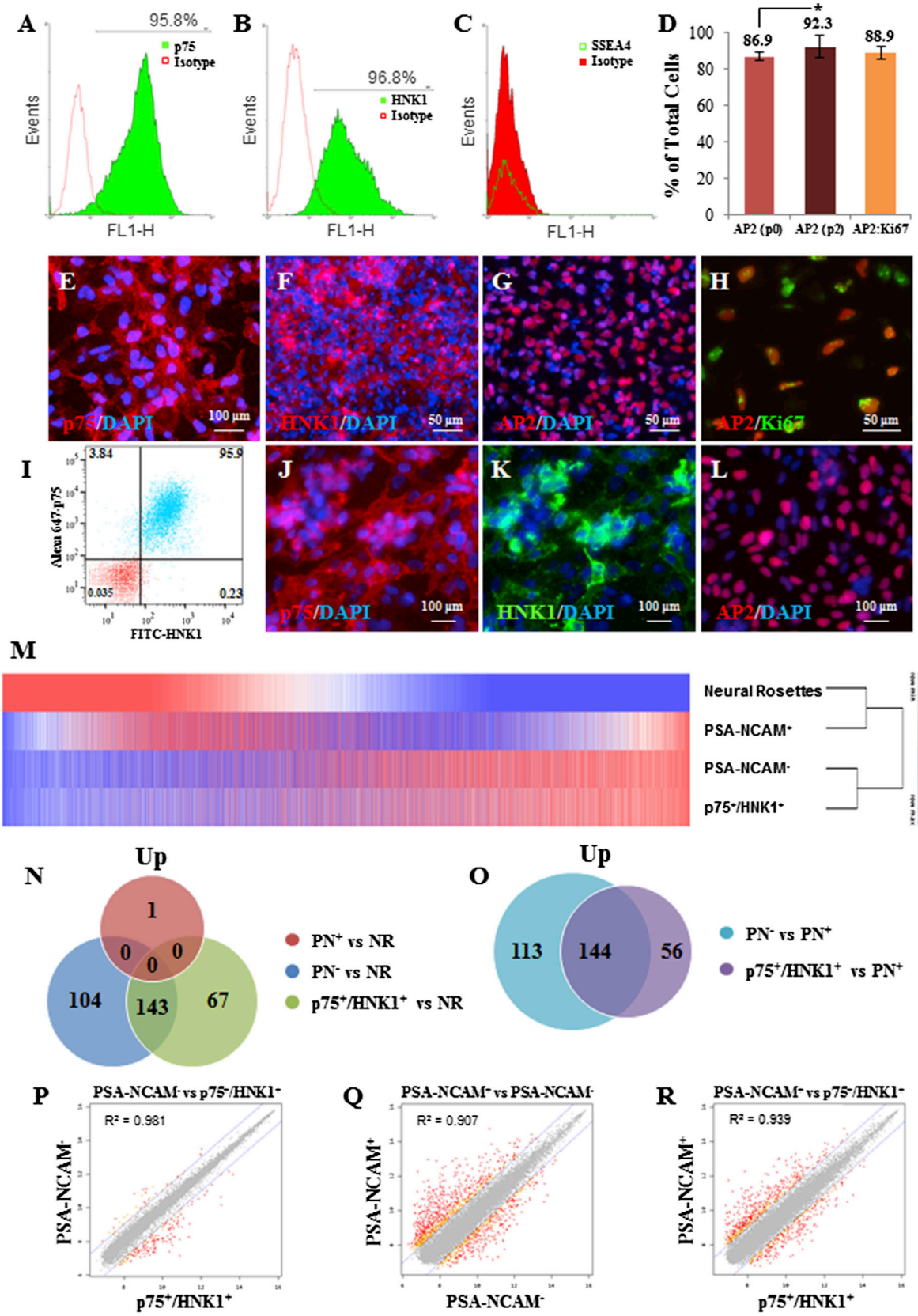

(legend on next page)

activated in PSA-NCAM$^-$ cells and 200 genes activated in p75$^+$/HNK1$^+$ cells identified a number of skeletal system-associated, neural tube-associated, mesenchyme-associated, and neural crest cell-associated terms (Tables 1, 2, S2, and S3). GO analysis also indicated that PSA-NCAM$^-$ and p75$^+$/HNK1$^+$ cells were more likely to undergo EMT in comparison to PSA-NCAM$^+$ cells (Tables S2 and S3). The scatter plots also showed that PSA-NCAM$^-$ and p75$^+$/HNK1$^+$ cells were the most similar of all the groups (Figures 2P–2R). In summary, the global gene expression profiles of PSA-NCAM$^-$ and p75$^+$/HNK1$^+$ cells revealed analogous molecular characteristics between the two groups in a comparison to PSA-NCAM$^+$, further confirming the authenticity of the NCSC characteristics of PSA-NCAN$^-$ cells.

Removal of PSA from PSA-NCAM$^+$ Cells or Low-Density Culture of PSA-NCAM$^+$ Cells Leads to Increased Neural Crest Cell Marker Expression

Our data demonstrate that PSA-NCAM$^-$ cells from neural rosette cultures are highly positive for neural crest markers. Although previous studies have taken advantage of PSA-NCAM expression to enrich NPCs or identify neuronal cells, they did not acknowledge the relationship between PSA-NCAM expression and the neural crest lineage of cells (Barral et al., 2013; Doi et al., 2012; Glaser et al., 2007; Kim et al., 2014). Based on a report suggesting PSA-NCAM involvement in the regulation of *p75* gene expression in subventricular zone-derived neurons (Gascon et al., 2007), we sought to examine the relationship between PSA-NCAM and p75$^+$ neural crest cell generation. We did not find any p75$^+$ neural crest cells in the PSA-NCAM$^+$ cell population (Figure S4A). However, unlike the glycerol control condition, p75$^+$ cells appeared after PSA-NCAM$^+$ cells were treated with endoneuraminidase-N (EndoN), an enzyme that specifically removes PSA from NCAM (Figures S4A–S4F). Conversely, treatment of PSA-NCAM$^-$ cells with either glycerol or EndoN did not alter the number of p75$^+$ cells (Figures S4G–S4L). Real-time RT-PCR analysis further confirmed that treatment of PSA-NCAM$^+$ cells with EndoN upregulated *p75* gene expression but did not enhance transcription of *ST8SIA2* and *ST8SIA4* genes encoding polysialyltransferases that are responsible for NCAM polysialylation (Figures S4M and S4N). Although removing PSA from PSA-NCAM$^+$ cells increased p75 expression, it did not affect the neural crest cell lineage-commitment process, showing no significant differences in the expression levels of other NCSC-related genes (Figure S4O). These results may suggest that any observed increase of p75 expression in PSA-NCAM$^+$ cells after PSA removal was not due to NCSC lineage commitment; rather, the PSA moiety of the PSA-NCAM protein negatively regulated *p75* gene expression, causing a lack of p75$^+$ neural crest cells in the PSA-NCAM$^+$ cell population. Thus, our data suggest an inverse relationship between PSA-NCAM and p75 during the neural induction process, thereby explaining why only PSA-NCAM$^-$ cells are highly positive for p75.

We also continued our investigation to determine whether that prolonged culture of positive or negative population leads to gradual accumulation or depletion of the NCSC population. Upon prolonged passaging of PSA-NCAM$^-$ cells, we did not observe morphological changes indicating the presence of neuroepithelial cells in the culture population (data not shown). However, we have noted the appearance of cells that resemble PSA-NCAM$^-$ cells in the positive culture population and noticed that the rate of NCSCs appearance increased based on the degree of confluence. Thus, we speculated that a cell density-dependent regulation might occur in

Figure 2. Molecular Characterization of PSA-NCAM$^-$ Cells and Global Gene Expression Pattern Analysis for PSA-NCAM$^{+/-}$ and p75$^+$/HNK1$^+$ Cells

(A and B) Flow cytometry analysis targeting p75 and HNK1 in PSA-NCAM$^-$ cells. Plots shown are representative of results from three different PSA-NCAM$^-$ cultures (n = 4).

(C) No SSEA4$^+$ cells were observed in PSA-NCAM$^-$ cells. The plot shown is representative of results from three different PSA-NCAM$^-$ cultures (n = 3).

(D) Within the PSA-NCAM$^-$ culture, 86.9% of unpassaged cells (p0) were AP2$^+$, and the positivity increased to 92.3% as the cells were passaged (p2); 88.9% of AP2$^+$ PSA-NCAM$^-$ cells were Ki67$^+$ (*$p < 0.05$, unpaired Student's t test, mean ± SEM, n = 3 independent experiments).

(E–H) Immunocytochemistry analysis of PSA-NCAM$^-$ cells showed strong expression of p75, HNK1, and AP2 with Ki67 activity.

(I–L) Validation of two step-MACS isolated p75$^+$/HNK1$^+$ cells via flow cytometry (95.9%) and immunocytochemistry analysis.

(M) Hierarchical clustering of the 20,287 genes was performed using the mean signal intensities of three biological replicates for each group (fail count < 6).

(N) Venn diagram of genes upregulated in PSA-NCAM$^+$, PSA-NCAM$^-$, and p75$^+$/HNK1$^+$ groups relative to the neural rosette group (PN$^+$, PSA-NCAM$^+$; PN$^-$, PSA-NCAM$^-$; and NR, neural rosettes).

(O) Genes with increased expression in the PSA-NCAM$^-$ and p75$^+$/HNK1$^+$ groups in a comparison to PSA-NCAM$^+$ group were compared using a Venn diagram.

(P–R) Scatter plots were drawn identifying r^2 values for each comparison.

See also Figures S2 and S3 and Table S1.

Table 1. Gene Ontology Analysis of 257 Genes Upregulated in PSA-NCAM$^-$ Cells Relative to PSA-NCAM$^+$ Cells

GO Accession Number	GO Term	Corrected p Value
GO: 0008284	positive regulation of cell proliferation	1.84E-08
GO: 0042127	regulation of cell proliferation	3.88E-08
GO: 0001501	skeletal system development	2.30E-07
GO: 0048705	skeletal system morphogenesis	7.02E-06
GO: 0048754	branching morphogenesis of a tube	1.11E-05
GO: 0035295	tube development	6.10E-05
GO: 0035239	tube morphogenesis	1.31E-04
GO: 0048706	embryonic skeletal system development	2.16E-03
GO: 0060562	epithelial tube morphogenesis	8.11E-03
GO: 0060348	bone development	1.54E-02
GO: 0002053	positive regulation of mesenchymal cell proliferation	1.68E-02
GO: 0010464	regulation of mesenchymal cell proliferation	1.88E-02
GO: 0048701	embryonic cranial skeleton morphogenesis	1.88E-02
GO: 0048762	mesenchymal cell differentiation	2.23E-02
GO: 0014031	mesenchymal cell development	2.23E-02
GO: 0060485	mesenchyme development	2.35E-02
GO: 0051216	cartilage development	5.73E-02
GO: 0014032	neural crest cell development	5.78E-02
GO: 0014033	neural crest cell differentiation	5.78E-02

See also Table S2.

Table 2. Gene Ontology Analysis of 200 Genes Upregulated in p75$^+$/HNK1$^+$ Cells Relative to PSA-NCAM$^+$ Cells

GO Accession Number	GO Term	Corrected p Value
GO: 0001501	skeletal system development	2.60E-10
GO: 0007389	pattern specification process	4.97E-08
GO: 0035295	tube development	2.29E-07
GO: 0035239	tube morphogenesis	4.42E-07
GO: 0042127	regulation of cell proliferation	5.40E-07
GO: 0048706	embryonic skeletal system development	7.94E-07
GO: 0008284	positive regulation of cell proliferation	1.23E-05
GO: 0048705	skeletal system morphogenesis	1.35E-05
GO: 0060485	mesenchyme development	1.47E-04
GO: 0048704	embryonic skeletal system morphogenesis	2.29E-04
GO: 0060562	epithelial tube morphogenesis	4.88E-04
GO: 0014031	mesenchymal cell development	1.52E-03
GO: 0048762	mesenchymal cell differentiation	1.52E-03
GO: 0014033	neural crest cell differentiation	4.00E-03
GO: 0014032	neural crest cell development	4.00E-03
GO: 0001843	neural tube closure	3.44E-02
GO: 0060606	tube closure	3.44E-02
GO: 0051216	cartilage development	3.56E-02
GO: 0014020	primary neural tube formation	4.10E-02
GO: 0001841	neural tube formation	5.79E-02

See also Table S3.

the PSA-NCAM$^+$ culture system. To investigate this further, we examined transcriptional changes of PSA-NCAM$^+$ cells (passages 4–8) in different density populations (cells/cm^2). Notably, expression levels of neural rosette-specific markers such as *PLZF* and *DASH1*, as well as neuroepithelial markers such as *PAX6* and *SOX1*, showed significant decreases in the lowest density of PSA-NCAM$^+$ cells (Figures S5A–S5D). Conversely, neural crest cell markers such as *AP2* and *p75* showed significant increases in the lowest density (Figures S5E and S5F). At a high density of PSA-NCAM$^+$ cells, 2.5 × 10^6 cells/cm^2, only SOX1$^+$ cells were observed with no appearance of AP2$^+$ cells. However, at a lowest density of PSA-NCAM$^+$ cells, 1.0 × 10^6 cells/cm^2, scattered AP2$^+$ cells were noted around SOX1$^+$ cells (Figure S5G). These data demonstrate that prolonged passaging of PSA-NCAM$^+$ cells at a high density is required to maintain neuroepithelial cell purity while minimizing the possible appearance of PSA-NCAM$^-$ cells.

PSA-NCAM$^-$ Cells Possess the Multilineage Differentiation Capacity of NCSCs

The neural crest is a multipotent population that originates from the dorsal region of the neural tube. NCSCs are multipotent and can differentiate into both ectodermal and mesodermal tissue lineages (Le Douarin and Dupin, 2003). To characterize the in vitro functionality of PSA-NCAM$^-$ cells, we promoted the differentiation of PSA-NCAM$^-$ cells into cells with a neural crest origin (Chimge and Bayarsaihan, 2010). Prior to inducing the multilineage differentiation of PSA-NCAM$^-$ cells, we ensured that there were no contaminating endodermal or mesodermal lineage cells. Neuroectoderm specified embryoid bodies (EBs) showed no contamination of endodermal and mesodermal

lineage cells prior to the PSA-NCAM$^-$-targeted sorting (Figures S6A and S6B). Thus, PSA-NCAM$^-$-derived mesodermal lineage cells during multilineage differentiation are solely dependent on PSA-NCAM$^-$ cell potency.

To examine whether PSA-NCAM$^-$ cells have the capacity to produce mesenchymal progenitors (MPs) mimicking neural crest development in vertebrates (Gammill and Bronner-Fraser, 2003; Sauka-Spengler and Bronner-Fraser, 2008; Theveneau and Mayor, 2012), we spontaneously differentiated the PSA-NCAM$^-$ cells by adding 10% fetal bovine serum (FBS) to the growth medium. Morphological changes were observed from day 4, and MPs appeared at day 14 (Figures 3A and 3B). Flow cytometry analysis at day 20 revealed the loss of p75 positivity in PSA-NCAM$^-$ cell-derived MPs, whereas mesenchymal markers such as CD44, CD29, CD73, CD105, and CD90 were detected (Figure 3C). To compare the ability to differentiate into mesenchymal lineages between PSA-NCAM$^-$ cells and p75$^+$/HNK1$^+$ cells, we performed real-time RT-PCR analysis targeting EMT markers such as *SNAIL*, *SLUG*, *TWIST1*, and *VIMENTIN*, as well as mesenchymal markers such as *CD29*, *CD44*, *CD73*, *CD90*, *CD105*, and *PDGFRα*. When the expression levels of both cell types exposed to 10% FBS were compared every 4 days for up to 32 days, no significant differences were observed (Figure S7A). The data suggest that both types of cells are capable of differentiating into MPs. PSA-NCAM$^+$ cells, on the other hand, failed to differentiate into mesenchymal lineages showing no significant increase in the expression levels of either EMT or mesenchymal markers but showed a decrease in cell viability when exposed to 10% FBS (Figures S7B–S7F).

We also determined that the MPs differentiated from PSA-NCAM$^-$ cells retained chondrogenic, osteogenic, and adipogenic differentiation potentials (Figures 3D–3F). The multipotency of NCSCs also includes differentiation into neurons that comprise the PNS. Late-passaged PSA-NCAM$^-$ cells (p6-p8) were induced to differentiate into PERIPHERIN$^+$ neurons via neuronal induction (Lee et al., 2010). NESTIN$^+$ PSA-NCAM$^-$ cells slowly lost their neural precursor characteristics and differentiated into TuJ1$^+$ neuronal cells (Figure 3G). PERIPHERIN$^+$ and TuJ1$^+$ PNS neurons were obtained on day 14 (Figure 3H). Finally, PSA-NCAM$^-$ cells could also differentiate into smooth muscle actin α (SMAα) and CALPONIN$^+$ smooth muscle cells (Figures 3I and 3J), further demonstrating the multipotentiality of PSA-NCAM$^-$ cells in vitro. Acquisition of mesenchymal features was also observed in iPSC-derived PSA-NCAM$^-$ cells (Figure S8A), and these cells could also differentiate into SMAα$^+$ and CALPONIN$^+$ cells (Figures S8B and S8C). Similar to bona fide neural crest cells in vivo, our data confirmed the multipotent behavior of PSA-NCAM$^-$ cells.

Tumors of Mesodermal Lineage, Pigmented Cells, and PERIPHERIN$^+$ Grafts Derived from PSA-NCAM$^-$ Cells

To characterize the cellular behavior of heterogeneous neural rosettes in vivo, we performed transplantations in adult rat brains. At 10 weeks post-transplantation, we observed rosette-rich neural overgrowth (Figures 4A–4C) and non-neuroectodermal origin grafts (Cocchia et al., 1983) such as a runt-related transcription factor 2 (RUNX2)$^+$ structure (Figures 4D and 4E). Rosette-forming neural overgrowth was identified in all transplanted animals (n = 8), while non-neuroectodermal structures with mesodermal lineages (referred to here as tumors) were developed in all but one of the animals (n = 7 of 8, 88%) (Figure 4F).

Previous studies that reported tumor formation following cell engraftment (Arnhold et al., 2004; Doi et al., 2012; Kim et al., 2012; Seminatore et al., 2010) and the fact that melanocytes, chondrocytes, and smooth muscle cells could be derived from NCSCs prompted us to examine whether PSA-NCAM$^-$ cells play a tumorigenic role when neural rosettes are used as a transplantation material. PSA-NCAM$^-$ cells were mixed with PSA-NCAM$^+$ cells at specific ratios and transplanted into the rat brain as follows: 100% PSA-NCAM$^-$ cells, 75% PSA-NCAM$^-$ cells/25% PSA-NCAM$^+$ cells, 25% PSA-NCAM$^-$ cells/75% PSA-NCAM$^+$ cells, and 100% PSA-NCAM$^+$ cells. Overall, 82%, 75%, and 57% of rats grafted with 100%, 75%, and 25% PSA-NCAM$^-$ cells developed tumors, respectively (Figure 4G). In contrast, neither tumor formation nor neural overgrowth was detected in animals grafted with 100% PSA-NCAM$^+$ cells. The grafts formed by the PSA-NCAM$^-$ cells also contained PERIPHERIN$^+$ cells and showed pigmentation as well as cyst formation (Figures 4H and 4I). Identified tumors were consisted of mesodermal lineage derivatives, such as RUNX2-expressing bone and SMAα-expressing smooth muscle tissues (Figures 4J and 4K). Representative H&E staining of rat brains revealed various mesodermal lineages but showed no endodermal lineage grafting (Figure 4L). While the 100% PSA-NCAM$^+$ cell grafts showed no sign of neural overgrowth or tumor formation (Figure 4M), the groups with PSA-NCAM$^-$ cells included in the grafts showed smooth muscle tissue, cyst formation, pigmentation, and prechondrogenic tissue (Figures 4N–4Q).

DISCUSSION

In this study, we analyzed the cause of mesodermal tumor development after CNS transplantation of neural rosette-NPCs. Our results demonstrate that the multipotent characteristics of NCSCs among the neural rosette populations are responsible for mesodermal tumor formation,

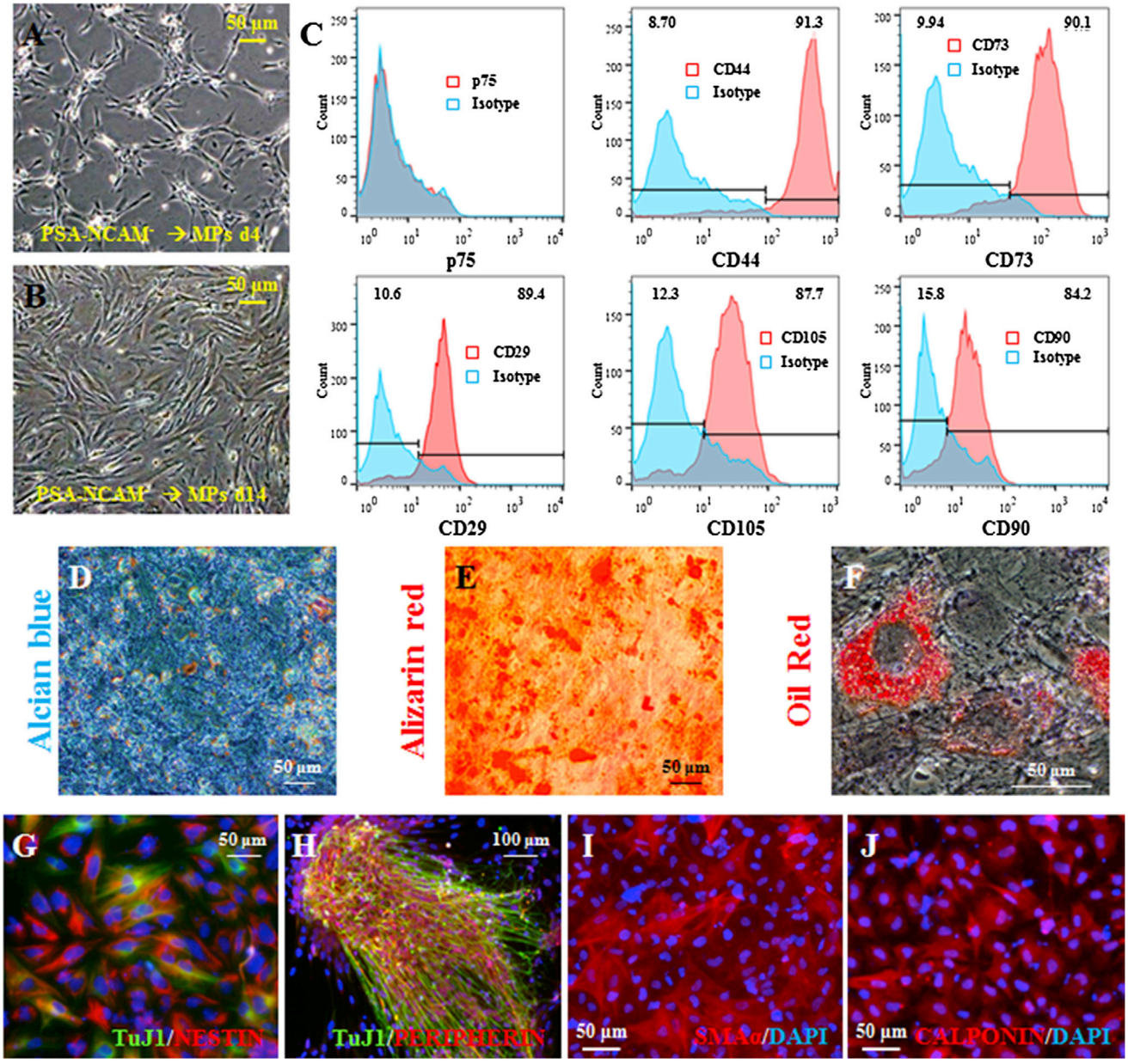

Figure 3. PSA-NCAM⁻ Cells Can Be Induced to Differentiate into Multilineages of NCSCs

(A and B) Bright-field images of MPs differentiated from PSA-NCAM⁻ (at d4 and d14).

(C) Loss of p75⁺ expression in PSA-NCAM⁻ cell-derived MPs. We also detected strong expression of mesenchymal cell markers, including CD44, CD29, CD73, CD105, and CD90. Plots shown are representative of results from three different PSA-NCAM⁻-derived MP cultures (n = 3).

(D–F) Generated MPs were further differentiated into the mesenchymal lineages including, Alcian blue-stained chondrocytes (D), Alizarin red-stained osteocytes (E), and Oil red O-stained adipocytes with oil droplets (red) (F).

(G and H) PSA-NCAM⁻ cells were induced to differentiate into PERIPHERIN⁺ neuronal cells. NESTIN⁺ PSA-NCAM⁻ cells were slowly lost but gained TuJ1 and PERIPHERIN positivity.

(I and J) SMAα^+ and CALPONIN⁺ smooth muscle cells were also obtained.

See also Figures S6–S8.

PERIPHERIN⁺ grafts, and the presence of pigmented cells. Thus, identifying surface markers such as PSA-NCAM that could distinguish between NPCs with CNS characteristics and NCSCs from neural rosette cell culture populations could reduce the tumorigenic potential of hPSC-derived NPCs.

We previously demonstrated that targeting PSA-NCAM$^+$ cells via MACS from neural rosettes obtained through dual-SMAD inhibition-induced neuralization could enrich NPCs up to 85% SOX1$^+$ cells (Kim et al., 2012). When these PSA-NCAM$^+$ sorted cells were further analyzed with FACS to confirm the MACS results, 93% of cells were PSA-NCAM$^+$. Meanwhile, our current study involved the expansion of neural rosettes obtained through the same method to produce a large number of cells for in vivo transplantation. According to our data (n = 4), the total neural rosette culture population after 7 days of expansion was 79% PSA-NCAM$^+$ cells and 21% PSA-NCAM$^-$ cells (Figure 1L).

Despite efforts to increase the efficiency of neural induction to achieve full neural conversion of hPSCs, the current dual-SMAD inhibition-induced neuralization method yields >80% PAX6$^+$ and 82% HES5$^+$ cells (Chambers et al., 2009) with >90% of total colonies containing neural rosettes (Kim et al., 2010). Although the ultimate goal would be to prevent NCSC development during the neural induction of hPSCs, this is challenging since NCSCs and SOX1$^+$/PAX6$^+$ neuroepithelial cells share the same major developmental signals, including bone morphogenetic proteins (BMPs), Wnt, fibroblast growth factor (FGF), and Notch signaling pathways (Basch and Bronner-Fraser, 2006). As a result, an elaborate differentiation method was required to increase the purity of SOX1$^+$/PAX6$^+$ neuroepithelial cells while suppressing NCSC development. The first approach was employed in a previous study and achieved a decrease of p75$^+$ cells after treatment with FGF and BMP antagonists (Lee et al., 2007). Although it may be possible to obtain >80% SOX1$^+$/PAX6$^+$ neuroepithelial cells via the initial isolation of neural rosettes, we would expect that the purity inevitably decreases during expansion to produce a large number of cells without any targeted cell sorting or antagonist treatment. Based on this information, we have concluded that 21% PSA-NCAM$^-$ cells in the neural rosette culture population was a reasonable proportion.

PSA-NCAM-targeted cell sorting from neural rosettes allowed an isolation of NCSC populations. Compared to the previously defined hPSC-derived NCSCs, p75$^+$/HNK1$^+$ cells, PSA-NCAM$^-$ cells exhibited similar molecular characteristics and multipotentiality; i.e., both were able to generate ectodermal and mesodermal lineages. We also identified an inverse relationship between PSA from NCAM and p75 in PSA-NCAM$^+$ cells. Removal of PSA from PSA-NCAM$^+$ cells with EndoN led to increased expression of the neural crest marker, p75, which explains enrichment of p75$^+$ cells in PSA-NCAM$^-$ populations (Figure S4). Though removing PSA from PSA-NCAM$^+$ cells showed no significant differences in the expression levels of NCSC-related genes other than *p75*, a hasty conclusion should not be made to exclude a possible role of PSA in NCSC lineage determination. Since our study targeted the removal of existing PSA from PSA-NCAM$^+$ cells in a short period of time, a loss-of-function study that acquires insights of protein function should be further considered to determine a role of PSA in NCSC lineage determination during the neural induction process.

Subsequent to PSA-NCAM-targeted cell sorting, in order to benefit from highly enriched PSA-NCAM$^+$ NPCs while shielded from PSA-NCAM$^-$ NCSCs, it is important to understand whether gradual accumulation or depletion of PSA-NCAM$^-$ NCSCs occurs in the PSA-NCAM$^+$ culture population upon prolonged passaging. We determined that a cell density-dependent regulation took place in the PSA-NCAM$^+$ culture system and the rate of NCSC appearance increased when the degree of confluence of positive cells decreased (Figure S5). Our data demonstrate that prolonged passaging of PSA-NCAM$^+$ cells at a high density is required to maintain neuroepithelial cell purity while minimizing the possible appearance of PSA-NCAM$^-$ cells. Although it has been determined that NCSCs originate from the border of neural and epidermal ectoderm based on "a long-standing interpretation" of developmental studies, it is still not clear whether NCSCs are induced or self-differentiated. If NCSCs are induced hypothetically, questions still remain whether their induction separates from, is part of, or occurs subsequent to the neural induction process of embryo (Hall, 2009). Thus, we cannot yet conclude whether appeared PSA-NCAM$^-$ cells in a low density of PSA-NCAM$^+$ cells were self-differentiated or induced from PSA-NCAM$^+$ cells at this point.

Previous studies targeted remaining PSCs in cell cultures in attempts to deplete tumor-initiating cells (Ben-David and Benvenisty, 2014; Tang et al., 2011). While such strategies were successful in removing PSCs, targeting PSCs alone was insufficient to completely eliminate tumorigenic potential of NPCs. Notably, our data indicate that isolated PSA-NCAM$^-$ cells play a significant role in mesodermal tumor development in the adult rat brain. The detection of mesodermal derivatives, PERIPHERIN$^+$ cells, and pigmented tissues in grafts of PSA-NCAM$^-$ cells suggested that tumorigenesis after neural rosette engraftment was caused by NCSCs that comprise the PSA-NCAM$^-$ cell population. Our results demonstrate that PSA-NCAM$^-$ NCSCs can be a critical target for tumor prevention in hPSC-derived-NPC-based therapy and suggest that removal of PSA-NCAM$^-$ cells would completely eliminate the tumorigenic potential originating from NCSCs following transplantation of NPCs into the CNS.

EXPERIMENTAL PROCEDURES

Stem Cell Culture and Differentiation

Undifferentiated hESCs (H9 [WA09; WiCell]) were cultured on mouse SIM Thioguanine/Ouabain-resistant mouse fibroblast cell

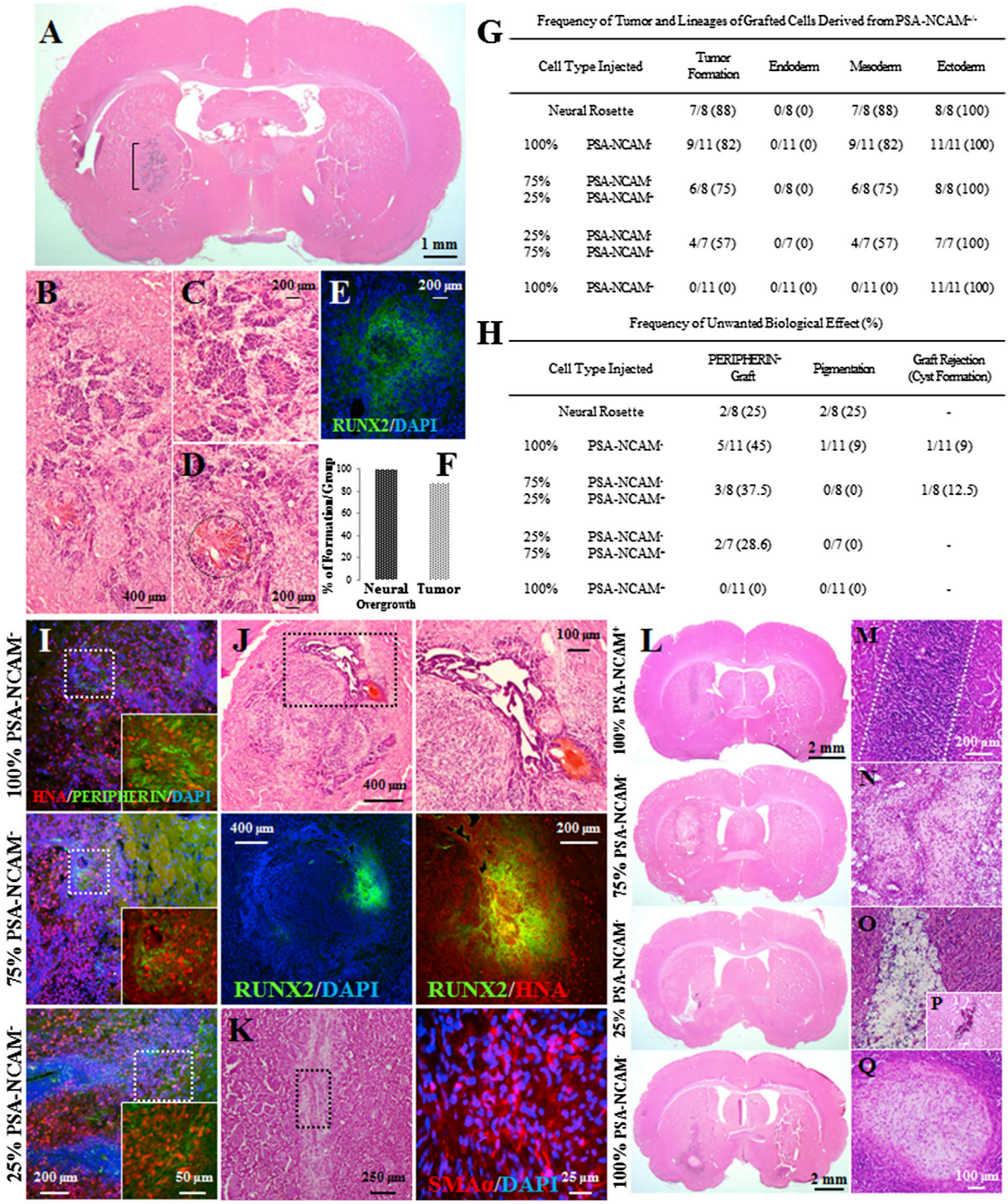

G

Frequency of Tumor and Lineages of Grafted Cells Derived from PSA-NCAM+/-

Cell Type Injected		Tumor Formation	Endoderm	Mesoderm	Ectoderm
Neural Rosette		7/8 (88)	0/8 (0)	7/8 (88)	8/8 (100)
100%	PSA-NCAM-	9/11 (82)	0/11 (0)	9/11 (82)	11/11 (100)
75% 25%	PSA-NCAM- PSA-NCAM+	6/8 (75)	0/8 (0)	6/8 (75)	8/8 (100)
25% 75%	PSA-NCAM- PSA-NCAM+	4/7 (57)	0/7 (0)	4/7 (57)	7/7 (100)
100%	PSA-NCAM+	0/11 (0)	0/11 (0)	0/11 (0)	11/11 (100)

H

Frequency of Unwanted Biological Effect (%)

Cell Type Injected		PERIPHERIN- Graft	Pigmentation	Graft Rejection (Cyst Formation)
Neural Rosette		2/8 (25)	2/8 (25)	-
100%	PSA-NCAM-	5/11 (45)	1/11 (9)	1/11 (9)
75% 25%	PSA-NCAM- PSA-NCAM+	3/8 (37.5)	0/8 (0)	1/8 (12.5)
25% 75%	PSA-NCAM- PSA-NCAM+	2/7 (28.6)	0/7 (0)	-
100%	PSA-NCAM+	0/11 (0)	0/11 (0)	-

Figure 4. Tumors of Mesodermal Lineage and PERIPHERIN$^+$ Grafts Can Be Derived from PSA-NCAM$^-$ Cells

(A–C) Representative H&E-stained neural rosette graft showing neural overgrowth.

(D and E) Structures of non-neuroectodermal origin such as RUNX2$^+$ graft.

(F) Neural overgrowth and tumor formation detected at rates of 100% and 88%, respectively, from neural rosette grafts.

(G) Summary of tumor formation and cell lineages derived from PSA-NCAM$^{+/-}$ grafts. Regardless of tumor formation, lineages were identified based on apparent phenotypes. Fractional numbers represent the number of rats identified with tumors or grafted cell lineages

(legend continued on next page)

line (STO) fibroblasts (ATCC) under previously described growth conditions (Jang et al., 2011). For induction of neural rosettes, EBs were cultured in suspension for 4 days in hESC media excluding basic FGF (bFGF) but supplemented with 5-μM dorsomorphin (DM) (Calbiochem) and 5- to 10-μM SB431542 (SB) (Sigma). On day 4, EBs were attached in Matrigel-coated culture dishes (BD Biosciences) in DMEM/F12 N2 supplemented media (N2 media) with 20-ng/ml bFGF (R&D Systems) and 19- to 21-μg/ml human insulin solution (Sigma-Aldrich) for another 5 days. The emerged rosette structures were mechanically isolated using pulled glass pipettes within the EB colonies, and isolated neural rosette clumps were replated in Matrigel-coated dishes. Replated neural rosettes were then expanded for an additional 6 to 7 days at 90% confluence. PSA-NCAM$^+$ and PSA-NCAM$^-$ cells were isolated via MACS (Miltenyi Biotec) as previously described (Kim et al., 2012). Isolated cells were plated in Matrigel-coated dishes at a density of 1–1.55 × 10^5 and 1–1.25 × 10^5 cells/cm^2 for PSA-NCAM$^+$ and PSA-NCAM$^-$ cells, respectively. Although PSA-NCAM$^-$ cells were maintained in N2 media with insulin, 20-ng/ml bFGF, and 10-ng/ml epidermal growth factor (EGF) (Peprotech), the positive cells were maintained in DMEM/F12 N2 and B27 without vitamin A-supplemented media (N2B27 media) with 20-ng/ml bFGF. Media were replaced daily. For isolation of NCSCs from the propagated neural rosette population, additional two-step MACS (CD271; CD57 MicroBeads, Miltenyi Biotec) was performed following the same procedures with a slight modification. Isolated CD271$^+$ cells were washed with calcium-, magnesium-free, and phenol red-free HBSS (GIBCO, Life Technologies) twice. The positive cells then eluted with 1 × TrypLE Express (GIBCO, Life Technologies) and nutated in TrypLE Express for 3–5 min (Lee and Lufkin, 2012). To stop the reaction, we washed cells with 2% BSA-PBS solution followed by 1× cold PBS wash before attachment of CD57 MicroBeads and application over a second column. For peripheral neuron differentiation, PSA-NCAM$^-$ cells (passages 6–8) were seeded in fibronectin- or poly-L-ornithine/laminin-coated four-well dishes in N2B27 media with brain-derived neurotrophic factor (10 ng/ml), glial cell line-derived neurotrophic factor (10 ng/ml), nerve growth factor (10 ng/ml), neurotrophin-3 (10 ng/ml) (all Peprotech), ascorbic acid (200 μM; Sigma-Aldrich), and N-[N-(3,5-Difluorophenacetyl)-L-alanyl]-S-phenylglycine t-butyl ester (DAPT) (2.5 μM; Calbiochem) (Lee et al., 2010). Differentiation was induced for 20 days before immunocytochemistry assays were performed. For mesenchymal differentiation, PSA-NCAM$^-$ cells were cultured in N2 media for 24 hr and switched to DMEM GlutaMAX supplemented with 10% FBS and 5-μg/ml gentamicin. Adipocyte, chondrocyte, and osteocyte differentiations were carried out according to the manufacturer's instructions using StemPro Differentiation Kits (Invitrogen). For removal of PSA from the surfaces, EndoN (Abc Scientific), which specifically degrades linear α-2,8-linked PSA, was introduced to PSA-NCAM$^{+/-}$ cells for 24 (data not shown) or 48 hr.

Immunocytochemistry and Flow Cytometry

Cells were fixed in 4% paraformaldehyde-PBS solution. For visualization of intracellular markers, cells were permeabilized with 0.1% Triton X-100-PBS solution, blocked with 2% BSA-PBS solution for 1 hr at room temperature, and incubated overnight at 4°C with primary antibodies as listed in Table S4. Appropriate fluorescence-tagged secondary antibodies (Molecular Probes and Vector Laboratories) were used for visualization. Cells were mounted in DAPI mounting medium (Vector Laboratories), and images were obtained using an Olympus IX71 microscope equipped with a DP71 digital camera or Olympus FSX100 system. MetaMorph Microscopy Automation and Image Analysis Software (Molecular Devices) were used to count positive cells in seven to ten randomly selected images at a final magnification of ×200 from each of three independent experiments. For flow cytometry, cells were dissociated into single cells using GIBCO Cell Dissociation Buffer (Invitrogen) and incubated in 1% BSA-PBS solution with the appropriate antibodies as listed in Table S4. For unconjugated primary antibodies, the cells were incubated with Alexa-Flour 488-conjugated anti-mouse IgG/IgM (Molecular Probes) for raising suitable secondary antibodies. Flow cytometry was performed using FACSCalibur (BD Biosciences) and analyzed using WinMDI 2.8 or FACSVerse (BD Biosciences) and FlowJo software.

Gene Expression Analyses and Transcription Profiling

Total RNA was isolated using the Easy-Spin Total RNA Extraction Kit (iNtRON). cDNA was synthesized from 1 μg of total RNA using

out of the total number of transplanted rats. The numbers in parentheses refer to percentage of rats identified with tumors or grafted cell lineages. Transplanted neural rosettes were derived from four independent experiments, while PSA-NCAM$^{+/-}$ cells were derived from five independent experiments, respectively.

(H) The frequencies of PERIPHERIN$^+$, pigmented graft detection, and cyst formation. Fractional numbers represent the number of rats identified with unwanted grafts out of the total number of transplanted rats. The numbers in parentheses refer to percentage of rats identified with unwanted grafts. Transplanted neural rosettes were derived from four independent experiments, while PSA-NCAM$^{+/-}$ cells were derived from five independent experiments, respectively.

(I) HNA$^+$/PERIPHERIN$^+$ cells in grafts with PSA-NCAM$^-$ cells.

(J) H&E staining and immunofluorescent histochemistry analysis showing RUNX2$^+$/HNA$^+$ bone tissue in PSA-NCAM$^-$ grafts.

(K) SMAα$^+$ smooth muscle tissue detected in PSA-NCAM$^-$ grafts.

(L) Representative H&E-stained coronal images revealing tumors of mesodermal lineage from PSA-NCAM$^-$ grafts (bottom three images) unlike the 100% PSA-NCAM$^+$ graft (top image).

(M) PSA-NCAM$^+$ cell graft showed no sign of neural overgrowth or tumor formation.

(N) The groups with PSA-NCAM$^-$ cell grafts showed smooth muscle tissue.

(O and P) Cyst formation and pigmentation observed in the groups with PSA-NCAM$^-$ cell grafts.

(Q) Prechondrogenic tissue formation observed in the groups with PSA-NCAM$^-$ cell grafts.

the PrimeScript RT Master Mix (Takara Bio). mRNA levels were quantified by real-time RT-PCR assays using the SYBR Premix Ex Taq (Takara Bio) and CFX96 Real-Time System (Bio-Rad). Ct values for each targeted gene were normalized according to those of β-actin, and the normalized expression levels of the targeted genes were compared between the sorted/unsorted samples and control samples based on the comparative Ct method. Data are expressed as the mean relative expression ± SEM from three independent experiments. Semiquantitative PCR was performed using the EmeraldAMP GT PCR master mix (Takara Bio) in the GeneAmp PCR System 2720 (Applied Biosystems). The sequences of the primers used to characterize H9, neural rosettes, and PSA-NCAM$^{+/-}$ cells are provided in Table S5. For microarray analysis, 10 μg of total RNA from each sample was processed and analyzed by Macrogen, and the samples were hybridized to the Human HT-12 Expression v.4.0 bead array. For clustering analysis, the normalized data were narrowed down to 20,287 using a cutoff based on fail count < 6. We found 1,178 out of 20,287 genes with $p > 0.05$ (local-pooled error test adjusted p value cutoff <0.05). GO analyses were performed using DAVID (Database for Annotation, Visualization and Integrated Discovery). Significantly upregulated genes were compared against DAVID's GO FAT database to clarify biological meanings. The p values were derived using Fisher's exact tests ($p < 0.01$; fold enrichment ≥ 2.0), and the corrected p values were applied to multiple testing corrections using the Benjamini-Yekutieli method.

In Vivo Transplantation and Immunohistochemistry

We used adult male Sprague-Dawley rats weighing 200–250 g at the time of transplantation (Orient Bio). Propagated neural rosettes (d7) and PSA-NCAM$^{+/-}$ cells were dissociated into single cells using Accutase (Millipore) and then suspended in Dulbecco's PBS to a final cell concentration of 1×10^5 cells/μl. Three microliters of the cell suspension was stereotaxically transplanted per rat at the following coordinates: AP +0.05, ML +0.30, DV −0.40 and −0.50. Next, 30-mg/kg Zoletil (Virbac) was combined with 10-mg/kg Rompun (Bayer) for anesthesia, and 10-mg/kg cyclosporine A (Chong Kun Dang) was intraperitoneally administered 24-hr pre-transplantation and every day thereafter until the rats were sacrificed. At 10 weeks post-transplantation, the rats were anesthetized with the anesthetic mixture (Zoletil:Rompun) and transcardially perfused with 0.9% saline solution followed by 4% paraformaldehyde. Removed brains were post-fixed overnight and cryoprotected in 30% sucrose-PBS solution. Cryoprotected brains were embedded in FSC 22 compound (Leica), and serial coronal sections were sliced at 16–20 μm using a cryostat (Thermo Scientific). Progressive H&E staining was performed, and immunohistochemistry was carried out as previously described (Kim et al., 2012). Lineages of structures found in each graft were determined based on H&E sections first, followed by immunofluorescence staining targeting specific antigens with appropriate antibodies as listed in Table S4. Animal research was conducted under the supervision of the Department of Laboratory Animal Medicine, Medical Research Center, Yonsei University College of Medicine and followed the guidelines of the Institutional Animal Care and Use Committee (Permit No. 2013-0040).

Statistical Analysis

Data are shown as the mean ± SEM of at least three independent experiments. Data were analyzed using the paired/unpaired, two-tailed Student's t tests or ANOVA when two or more groups were involved.

ACCESSION NUMBERS

The accession number for the microarray data reported in this study is GEO: GSE67383.

SUPPLEMENTAL INFORMATION

Supplemental Information includes eight figures and five tables and can be found with this article online at http://dx.doi.org/10.1016/j.stemcr.2015.04.002.

AUTHOR CONTRIBUTIONS

D.R.L. participated in study conception and design; hPSC differentiation; cellular/molecular assays; rat transplantation; histological analyses; data assembly, analysis, and interpretation; and manuscript writing. J.-E.Y., J.S.L., S.P., J.L., and E.J. provided hPSC differentiation and cellular/molecular assays. C.-Y.P. helped with iPSC clone derivation, maintenance, and validation. H.-S.K. and D.-Y.H. were in charge of data interpretation. D.-S.K. provided study conception and design, data analysis and interpretation, and manuscript writing. D.-W.K. offered study conception, data analysis and interpretation, and manuscript writing.

ACKNOWLEDGMENTS

D.-W.K. was supported by National Research Foundation of Korea Bio and Medical Technology Development Program Grants 2012M3A9B4028631 and 2012M3A9C7050126 and by Korean Ministry of Health and Welfare Grant A120254.

Received: October 10, 2014
Revised: April 1, 2015
Accepted: April 2, 2015
Published: April 30, 2015

REFERENCES

Arnhold, S., Klein, H., Semkova, I., Addicks, K., and Schraermeyer, U. (2004). Neurally selected embryonic stem cells induce tumor formation after long-term survival following engraftment into the subretinal space. Invest. Ophthalmol. Vis. Sci. *45*, 4251–4255.

Barral, S., Ecklebe, J., Tomiuk, S., Tiveron, M.C., Desoeuvre, A., Eckardt, D., Cremer, H., and Bosio, A. (2013). Efficient neuronal in vitro and in vivo differentiation after immunomagnetic purification of mESC derived neuronal precursors. Stem Cell Res. (Amst.) *10*, 133–146.

Basch, M.L., and Bronner-Fraser, M. (2006). Neural crest inducing signals. Adv. Exp. Med. Biol. *589*, 24–31.

Ben-David, U., and Benvenisty, N. (2014). Chemical ablation of tumor-initiating human pluripotent stem cells. Nat. Protoc. *9*, 729–740.

Chambers, S.M., Fasano, C.A., Papapetrou, E.P., Tomishima, M., Sadelain, M., and Studer, L. (2009). Highly efficient neural conversion of human ES and iPS cells by dual inhibition of SMAD signaling. Nat. Biotechnol. *27*, 275–280.

Chimge, N.O., and Bayarsaihan, D. (2010). Generation of neural crest progenitors from human embryonic stem cells. J. Exp. Zool. B Mol. Dev. Evol. *314*, 95–103.

Cocchia, D., Polak, J.M., Terenghi, G., Battaglia, F., Stolfi, V., Gangitano, C., and Michetti, F. (1983). Localization of S-100 protein in Müller cells of the retina—2. Electron microscopical immunocytochemistry. Invest. Ophthalmol. Vis. Sci. *24*, 980–984.

Conti, L., and Cattaneo, E. (2010). Neural stem cell systems: physiological players or in vitro entities? Nat. Rev. Neurosci. *11*, 176–187.

Doi, D., Morizane, A., Kikuchi, T., Onoe, H., Hayashi, T., Kawasaki, T., Motono, M., Sasai, Y., Saiki, H., Gomi, M., et al. (2012). Prolonged maturation culture favors a reduction in the tumorigenicity and the dopaminergic function of human ESC-derived neural cells in a primate model of Parkinson's disease. Stem Cells *30*, 935–945.

Elkabetz, Y., Panagiotakos, G., Al Shamy, G., Socci, N.D., Tabar, V., and Studer, L. (2008). Human ES cell-derived neural rosettes reveal a functionally distinct early neural stem cell stage. Genes Dev. *22*, 152–165.

Gammill, L.S., and Bronner-Fraser, M. (2003). Neural crest specification: migrating into genomics. Nat. Rev. Neurosci. *4*, 795–805.

Gascon, E., Vutskits, L., Jenny, B., Durbec, P., and Kiss, J.Z. (2007). PSA-NCAM in postnatally generated immature neurons of the olfactory bulb: a crucial role in regulating p75 expression and cell survival. Development *134*, 1181–1190.

Glaser, T., Brose, C., Franceschini, I., Hamann, K., Smorodchenko, A., Zipp, F., Dubois-Dalcq, M., and Brüstle, O. (2007). Neural cell adhesion molecule polysialylation enhances the sensitivity of embryonic stem cell-derived neural precursors to migration guidance cues. Stem Cells *25*, 3016–3025.

Hall, B.K. (2009). The Neural Crest and Neural Crest Cells in Vertebrate Development and Evolution, Second Edition (New York: Springer).

Jang, J., Kang, H.C., Kim, H.S., Kim, J.Y., Huh, Y.J., Kim, D.S., Yoo, J.E., Lee, J.A., Lim, B., Lee, J., et al. (2011). Induced pluripotent stem cell models from X-linked adrenoleukodystrophy patients. Ann. Neurol. *70*, 402–409.

Jiang, X., Gwye, Y., McKeown, S.J., Bronner-Fraser, M., Lutzko, C., and Lawlor, E.R. (2009). Isolation and characterization of neural crest stem cells derived from in vitro-differentiated human embryonic stem cells. Stem Cells Dev. *18*, 1059–1070.

Kim, D.S., Lee, J.S., Leem, J.W., Huh, Y.J., Kim, J.Y., Kim, H.S., Park, I.H., Daley, G.Q., Hwang, D.Y., and Kim, D.W. (2010). Robust enhancement of neural differentiation from human ES and iPS cells regardless of their innate difference in differentiation propensity. Stem Cell Rev. *6*, 270–281.

Kim, D.S., Lee, D.R., Kim, H.S., Yoo, J.E., Jung, S.J., Lim, B.Y., Jang, J., Kang, H.C., You, S., Hwang, D.Y., et al. (2012). Highly pure and expandable PSA-NCAM-positive neural precursors from human ESC and iPSC-derived neural rosettes. PLoS ONE *7*, e39715.

Kim, H.S., Choi, S.M., Yang, W., Kim, D.S., Lee, D.R., Cho, S.R., and Kim, D.W. (2014). PSA-NCAM(+) neural precursor cells from human embryonic stem cells promote neural tissue integrity and behavioral performance in a rat stroke model. Stem Cell Rev. *10*, 761–771.

Kirkeby, A., Grealish, S., Wolf, D.A., Nelander, J., Wood, J., Lundblad, M., Lindvall, O., and Parmar, M. (2012). Generation of regionally specified neural progenitors and functional neurons from human embryonic stem cells under defined conditions. Cell Rep. *1*, 703–714.

Knecht, A.K., and Bronner-Fraser, M. (2002). Induction of the neural crest: a multigene process. Nat. Rev. Genet. *3*, 453–461.

Koch, P., Opitz, T., Steinbeck, J.A., Ladewig, J., and Brüstle, O. (2009). A rosette-type, self-renewing human ES cell-derived neural stem cell with potential for in vitro instruction and synaptic integration. Proc. Natl. Acad. Sci. USA *106*, 3225–3230.

Kreitzer, F.R., Salomonis, N., Sheehan, A., Huang, M., Park, J.S., Spindler, M.J., Lizarraga, P., Weiss, W.A., So, P.L., and Conklin, B.R. (2013). A robust method to derive functional neural crest cells from human pluripotent stem cells. Am. J. Stem Cells *2*, 119–131.

Kriks, S., Shim, J.W., Piao, J., Ganat, Y.M., Wakeman, D.R., Xie, Z., Carrillo-Reid, L., Auyeung, G., Antonacci, C., Buch, A., et al. (2011). Dopamine neurons derived from human ES cells efficiently engraft in animal models of Parkinson's disease. Nature *480*, 547–551.

Le Douarin, N.M., and Dupin, E. (2003). Multipotentiality of the neural crest. Curr. Opin. Genet. Dev. *13*, 529–536.

Lee, M.Y., and Lufkin, T. (2012). Development of the "Three-step MACS": a novel strategy for isolating rare cell populations in the absence of known cell surface markers from complex animal tissue. J. Biomol. Tech. *23*, 69–77.

Lee, G., Kim, H., Elkabetz, Y., Al Shamy, G., Panagiotakos, G., Barberi, T., Tabar, V., and Studer, L. (2007). Isolation and directed differentiation of neural crest stem cells derived from human embryonic stem cells. Nat. Biotechnol. *25*, 1468–1475.

Lee, G., Chambers, S.M., Tomishima, M.J., and Studer, L. (2010). Derivation of neural crest cells from human pluripotent stem cells. Nat. Protoc. *5*, 688–701.

Liu, Y., Weick, J.P., Liu, H., Krencik, R., Zhang, X., Ma, L., Zhou, G.M., Ayala, M., and Zhang, S.C. (2013). Medial ganglionic eminence-like cells derived from human embryonic stem cells correct learning and memory deficits. Nat. Biotechnol. *31*, 440–447.

Menendez, L., Yatskievych, T.A., Antin, P.B., and Dalton, S. (2011). Wnt signaling and a Smad pathway blockade direct the differentiation of human pluripotent stem cells to multipotent neural crest cells. Proc. Natl. Acad. Sci. USA *108*, 19240–19245.

Prasad, M.S., Sauka-Spengler, T., and LaBonne, C. (2012). Induction of the neural crest state: control of stem cell attributes by gene regulatory, post-transcriptional and epigenetic interactions. Dev. Biol. *366*, 10–21.

Sauka-Spengler, T., and Bronner-Fraser, M. (2008). A gene regulatory network orchestrates neural crest formation. Nat. Rev. Mol. Cell Biol. *9*, 557–568.

Seminatore, C., Polentes, J., Ellman, D., Kozubenko, N., Itier, V., Tine, S., Tritschler, L., Brenot, M., Guidou, E., Blondeau, J., et al.

(2010). The postischemic environment differentially impacts teratoma or tumor formation after transplantation of human embryonic stem cell-derived neural progenitors. Stroke *41*, 153–159.

Tang, C., Lee, A.S., Volkmer, J.P., Sahoo, D., Nag, D., Mosley, A.R., Inlay, M.A., Ardehali, R., Chavez, S.L., Pera, R.R., et al. (2011). An antibody against SSEA-5 glycan on human pluripotent stem cells enables removal of teratoma-forming cells. Nat. Biotechnol. *29*, 829–834.

Theveneau, E., and Mayor, R. (2012). Neural crest migration: interplay between chemorepellents, chemoattractants, contact inhibition, epithelial-mesenchymal transition, and collective cell migration. Wiley Interdiscip. Rev. Dev. Biol. *1*, 435–445.